Hindawi Publishing Corporation
Evidence-Based Complementary and Alternative Medicine
Volume 2011, Article ID 157090, 6 pages
doi:10.1155/2011/157090

Research Article

Short-Term Effects of Acupuncture on Open-Angle Glaucoma in Retrobulbar Circulation: Additional Therapy to Standard Medication

Shin Takayama,[1] Takashi Seki,[1] Toru Nakazawa,[2] Naoko Aizawa,[2] Seri Takahashi,[2] Masashi Watanabe,[1] Masayuki Izumi,[1] Soichiro Kaneko,[1] Tetsuharu Kamiya,[1] Ayane Matsuda,[1] Akiko Kikuchi,[1] Tomoyuki Yambe,[3] Makoto Yoshizawa,[4] Shin-ichi Nitta,[3] and Nobuo Yaegashi[1]

[1] *Department of Traditional Asian Medicine, Graduate School of Medicine, Tohoku University, 1-1 Seiryo-machi, Aoba-ku, Sendai, Miyagi 980-8574, Japan*
[2] *Department of Ophthalmology and Visual Science, Graduate School of Medicine, Tohoku University, Sendai 980-8574, Japan*
[3] *Institute of Development, Aging and Cancer, Tohoku University, Sendai 980-8575, Japan*
[4] *Research Division on Advanced Information Technology, Cyberscience Center, Tohoku University, Japan*

Correspondence should be addressed to Takashi Seki, t-seki@m.tohoku.ac.jp

Received 29 October 2010; Revised 7 December 2010; Accepted 11 January 2011

Background. The relation between glaucoma and retrobulbar circulation in the prognosis has been indicated. *Purpose.* To investigate the effects of acupuncture on retrobulbar circulation in open-angle glaucoma (OAG) patients. *Methods.* Eleven OAG patients (20 eyes with OAG) who were treated by topical antiglaucoma medications for at least 3 months were enrolled. Acupuncture was performed once at acupoints BL2, M-HN9, ST2, ST36, SP6, KI3, LR3, GB20, BL18, and BL23 bilaterally. Retrobulbar circulation was measured with color Doppler imaging, and intraocular pressure (IOP) was also measured at rest and one hour after rest or before and after acupuncture. *Results.* The Δ value of the resistive index in the short posterior ciliary artery ($P < .01$) and the Δ value of IOP ($P < .01$) were decreased significantly by acupuncture compared with no acupuncture treatment. *Conclusions.* Acupuncture can improve the retrobulbar circulation and IOP, which may indicate the efficacy of acupuncture for OAG.

1. Introduction

Glaucoma is one of the causes of blindness [1] and the Tajimi Study showed that the prevalence of primary open-angle glaucoma (OAG) was 3.9% in Japan [2]. The main treatment strategy of glaucoma is to control the intraocular pressure (IOP) [3]. Although IOP reduction is currently the main target for the treatment of glaucoma, treatment modalities that enhance retrobulbar hemodynamics in addition to reducing IOP may have a beneficial effect on the glaucoma therapy. It has been reported that glaucoma is associated with reduction in the blood flow velocity and elevation of the resistive index (RI) in the retrobulbar vessels [4–7]. It has also been reported that patients with OAG have impaired hemodynamics in ophthalmic circulation [8–10]. The impaired ocular circulation contributes to the progression of glaucomatous damage [11–13]. Therefore, new drugs or interventions that improve ocular hemodynamics may be preferable.

Recently, acupuncture has been widely applied to treat several conditions such as neck pain, shoulder pain, lumbar pain, headache, and hypertension in Asian and Western countries, and it has also been found to be effective for many conditions in several randomized trials [14–20]. Acupuncture has also been used for the treatment of ocular diseases, including glaucoma, in traditional Chinese medicine [21]. We have shown that acupuncture therapy added to the standard medication could affect the IOP level in eyes with normal-tension glaucoma [22], and several other studies have demonstrated that

acupuncture improves choroidal blood flow in the eye [23–25].

We have already reported that color Doppler imaging (CDI) by ultrasound is suitable for measuring the blood flow change in several organs during traditional Chinese medicine therapy [26–30]. The real-time and noninvasive hemodynamic measurement with CDI has been applied for measuring the retrobulbar vessel hemodynamics, and the reproducibility has already been shown [31]. In this study, we evaluate the hemodynamic changes in retrobulbar vessels by CDI to investigate the effect of acupuncture on OAG eyes.

2. Subjects

After the ethics committee approved the study, 11 patients diagnosed with OAG (20 eyes with OAG) were enrolled in this study. The patients received standard medical treatment for at least 3 months. The patients who had an experience of laser trabeculoplasty, any ocular surgery, or inflammation within the past year were excluded in the present study.

Table 1: Characteristic data of the patients with open-angle glaucoma.

Variable	Value
Number of patients	11
Age (years)	63 ± 11
Sexuality (male, female)	(1, 10)
Number of eyes with glaucoma	20
Best corrected visual acuity	1.1 ± 0.3
Spherical equivalent (D)	−1.6 ± 3.2
Humphrey automated perimeter	
Mean deviation (dB)	−11.5 ± 7.8
Pattern standard deviation (dB)	10.2 ± 4.5
OCT RNFL thickness (μm)	70.5 ± 21.8
The number of topical medications	
None	1
One kind	4
Two kinds	1
More than three kinds	5

3. Methods

3.1. Acupuncture. On the trial days, the patients arrived under regular medications. They received acupuncture therapy as follows in the morning. The acupoints were selected on the basis of the principles of traditional Chinese medicine. Acupuncture was performed for 15 min using disposable stainless steel needles (0.16 mm or 0.20 mm × 40 mm; Seirin Co. Ltd., Shizuoka, Japan) at acupoints Cuanzhu (BL2), Taiyang (M-HN9), Sibai (ST2), Zusanli (ST36), Sanyinjiao (SP6), Taixi (KI3), and Taichong (LR3) bilaterally while the patient was in the supine position and at acupoints Fengchi (GB20), Ganshu (BL18), and Shenshu (BL23) bilaterally while the patient was in the prone position for 15 min. Each needle was simply inserted without any intention of eliciting specific responses (e.g., de-qi feelings) to a depth of approximately 20 mm at acupoints ST36, SP6, KI3, GB20, BL18, and BL23. For acupoints BL2, M-HN9, ST2, and LR3, the needles were inserted to a depth of approximately 3–10 mm. Neither needle manipulation techniques nor other auxiliary interventions were used. Five licensed acupuncturists and one physician-acupuncturist with over 5 years of acupuncture experience administered the acupuncture treatment.

3.2. Measurements. To minimize the effects of diurnal variation, all measurements were recorded at the same time of the day (between 10 AM and 11 AM) for each patient by the same examiner. As a control, the subjects received the measurements of the systemic hemodynamics, retrobulbar vessel hemodynamics, and IOP that were performed at rest and one hour after rest. One month later, they received the same measurements before and after acupuncture treatment. The systemic hemodynamics was measured by an oscillometer and the hemodynamics in retrobulbar vessels was measured by ultrasound (LOGIQ e, GE Healthcare, Tokyo, Japan). The ultrasound measurements were performed after 10-minute rest in an air-conditioned room, avoiding any pressure on the eye, with the patients in the supine position. CDI was performed with a 13 MHz linear transducer for retrobulbar vessels such as the ophthalmic artery (OA), central retinal artery (CRA), and short posterior ciliary artery (SPCA). The OA was examined approximately 20 mm behind the globe (Figure 1(a)), the CRA was examined within 5 mm of the retrolaminar portion of the optic nerve (Figure 1(b)), and the temporal SPCA was examined approximately 5–10 mm behind the globe (Figure 1(c)). All blood flow velocity waveforms were measured at the corrected Doppler angle. Resistive index (RI: (peak systolic velocity − end-diastolic velocity)/peak systolic velocity) was also measured in each retrobulbar vessel.

3.3. Statistical Analysis. Statistical analysis was performed with the SPSS software (version 16.0, SPSS Japan Inc., Tokyo, Japan). The parameters between before and after acupuncture or between control and acupuncture were compared by paired t-test.

4. Results

Table 1 shows the characteristics of the subjects. One male and ten female glaucoma patients with a mean age of 63 ± 11 years were observed. The systemic hemodynamic parameters including heart rate, blood pressure, and IOP are shown in Table 2. The blood pressure and heart rate did not change significantly by acupuncture.

The IOP level significantly decreased by acupuncture compared with before acupuncture ($P < .05$). The Δ value of IOP also significantly decreased by acupuncture compared with control ($P < .01$) (Table 2).

Retrobulbar vessel RI in the OA, CRA, and SPCA is shown in Table 3. The RI in the CRA and SPCA decreased

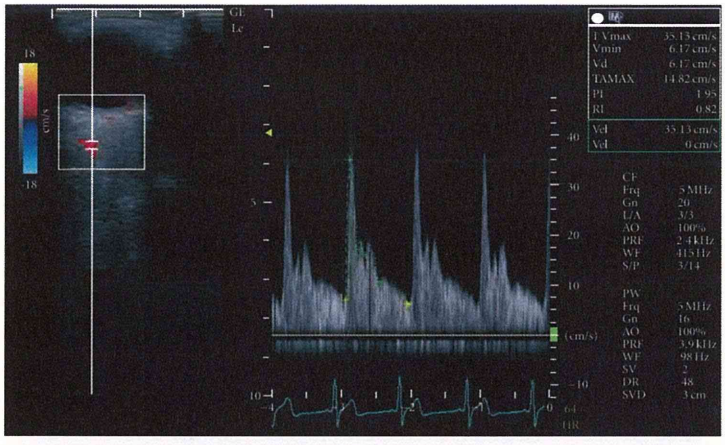

(a)

(b)

(c)

Figure 1: Horizontal scans by color Doppler imaging through the globe showing the (a) ophthalmic artery, (b) central retinal artery, and (c) short posterior ciliary artery.

Table 2: Blood pressure, heart rate, and intraocular pressure in control and acupuncture therapy. The values represent the mean and SD. $^{*}P < .05$, $^{**}P < .01$ versus rest or before acupuncture. $^{\dagger}P < .05$, $^{\dagger\dagger}P < .01$ versus control.

Parameter	Control			Acupuncture		
	Rest	After 1 hour	Δ value	Before	After	Δ value
Systole blood pressure (mm Hg)	116.4 ± 10.0	119.8 ± 7.6	3.4 ± 7.4	124.5 ± 12.9	122.6 ± 9.7	−1.1 ± 7.9
Diastolic blood pressure (mm Hg)	69.8 ± 6.5	68.6 ± 3.9	−1.0 ± 9.4	74.5 ± 5.4	72.0 ± 2.9	−3.0 ± 5.5
Heart rate (beats/min)	61.5 ± 7.3	60.1 ± 8.1	−2.5 ± 3.8	61.7 ± 8.5	60.3 ± 10.4	−2.4 ± 5.5
Intraocular pressure (mm Hg)	16.0 ± 4.1	17.1 ± 4.2**	1 ± 0.9	17.0 ± 5.0	16.0 ± 4.3*	−1 ± 1.9††

Table 3: Resistive index (RI) in the ophthalmic artery, central retinal artery, and short posterior ciliary artery. The values represent the mean and SD. $^{*}P < .05$, $^{**}P < .01$ versus before acupuncture. $^{\dagger}P < .05$, $^{\dagger\dagger}P < .01$ versus control.

Resistive index	Control			Acupuncture		
	Rest	After 1 hour	Δ value	Before	After	Δ value
Ophthalmic artery	0.74 ± 0.04	0.75 ± 0.05	0.006 ± 0.037	0.74 ± 0.04	0.74 ± 0.04	−0.006 ± 0.036
Central retinal artery	0.75 ± 0.09	0.72 ± 0.03	−0.027 ± 0.085	0.72 ± 0.05	0.68 ± 0.04*	−0.036 ± 0.059
Short posterior ciliary artery	0.68 ± 0.05	0.68 ± 0.04	0.004 ± 0.038	0.67 ± 0.04	0.64 ± 0.06*	−0.032 ± 0.054††

significantly by acupuncture compared with before acupuncture ($P < .05$). The Δ value of RI in the SPCA also significantly decreased by acupuncture compared with control ($P < .01$) (Table 3).

5. Discussion

To our best knowledge, this is the first report on hemodynamic change in retrobulbar vessels related to acupuncture in OAG eyes. The present findings suggest that acupuncture can alter vessel resistance in the SPCA, even though the eyes are treated with standard medications.

The OA originates from the internal carotid artery. The CRA and SPCA are the ocular branches of the OA [32]. The CRA supplies blood to the retina and SPCA, to the choroid. CDI by ultrasound is useful for the measurement of the blood flow in various vessels in real time. Since it is impossible to determine the diameter of very small retrobulbar vessels, CDI cannot directly measure blood flow volume. However, the decrease of the distal vascular resistance in the SPCA indicates an increase of the blood flow in the choroid. We have already reported that acupuncture could increase the blood flow volume in the upper limb without an increase in the cardiac output, and the increased reaction in the blood flow was mediated by the decrease in the vascular resistance on the basis of the decreased vascular tone [30]. The mechanisms by which acupuncture can alter retrobulbar vessel circulation are still unclear. However, it has been reported that the blood flow in the eye is controlled by sympathetic and parasympathetic nerves, and it is related with the release of nitric oxide or calcitonin gene-related peptide [33, 34]; it has also been reported that the regulation of regional blood flow by somatic afferent stimulation is based on somatoautonomic reflex mechanisms in the choroidal blood flow of the eyeball [34]. The hemodynamic changes in the SPCA by acupuncture may be related with these mechanisms. Reduced blood flow velocities and increased vascular resistance in the retrobulbar arteries appear to be a risk factor for glaucoma progression [35–38]. Thus, acupuncture may be applied for additional therapy to treat OAG.

We should view these results cautiously because the present study was a case series study and intervention was provided only once. Longer observation of acupuncture therapy is needed to investigate the progression of glaucomatous damage associated with impaired ocular circulation.

6. Conclusions

The vessel resistance in the SPCA and the IOP level were decreased by acupuncture in OAG eyes. Acupuncture can affect the retrobulbar circulation and IOP despite the administration of standard medication. The present study implies the possibility that acupuncture is effective for OAG with standard medication.

Acknowledgment

This work was supported by Health and Labour Sciences Research Grants for Clinical Research from the Japanese Ministry of Health, Labour and Welfare.

References

[1] K. Nakae, K. Masuda, T. Aneo et al., "Wagakuni ni okeru shiryokushougai no genjou," *Research Committee on Chorioretinal Degenerations and Optic Atrophy, the Ministry of Health, Labour and Welfare of Japan*, vol. 17, pp. 263–276, 2005.

[2] A. Iwase, Y. Suzuki, M. Araie et al., "The prevalence of primary open-angle glaucoma in Japanese: the Tajimi study," *Ophthalmology*, vol. 111, no. 9, pp. 1641–1648, 2004.

[3] R. N. Weinreb and P. Tee Khaw, "Primary open-angle glaucoma," *The Lancet*, vol. 363, no. 9422, pp. 1711–1720, 2004.

[4] C. Akarsu and M. Y. K. Bilgili, "Color Doppler imaging in ocular hypertension and open-angle glaucoma," *Graefe's*

Archive for Clinical and Experimental Ophthalmology, vol. 242, no. 2, pp. 125–129, 2004.

[5] V. P. Costa, A. Harris, E. Stefánsson et al., "The effects of antiglaucoma and systemic medications on ocular blood flow," *Progress in Retinal and Eye Research*, vol. 22, no. 6, pp. 769–805, 2003.

[6] H. J. Kaiser, A. Schoetzau, D. Stumpfig, and J. Flammer, "Blood-flow velocities of the extraocular vessels in patients with high- tension and normal-tension primary open-angle glaucoma," *American Journal of Ophthalmology*, vol. 123, no. 3, pp. 320–327, 1997.

[7] S. J. A. Rankin, "Color Doppler imaging of the retrobulbar circulation in glaucoma," *Survey of Ophthalmology*, vol. 43, no. 1, pp. S176–S182, 1999.

[8] I. Stalmans, A. Harris, S. Fieuws et al., "Color Doppler imaging and ocular pulse amplitude in glaucomatous and healthy eyes," *European Journal of Ophthalmology*, vol. 19, no. 4, pp. 580–587, 2009.

[9] I. Janulevičiene, I. Sliesoraityte, B. Siesky, and A. Harris, "Diagnostic compatibility of structural and haemodynamic parameters in open-angle glaucoma patients," *Acta Ophthalmologica*, vol. 86, no. 5, pp. 552–557, 2008.

[10] N. Plange, M. Kaup, O. Arend, and A. Remky, "Asymmetric visual field loss and retrobulbar haemodynamics in primary open-angle glaucoma," *Graefe's Archive for Clinical and Experimental Ophthalmology*, vol. 244, no. 8, pp. 978–983, 2006.

[11] M. Satilmis, S. Orgül, B. Doubler, and J. Flammer, "Rate of progression of glaucoma correlates with retrobulbar circulation and intraocular pressure," *American Journal of Ophthalmology*, vol. 135, no. 5, pp. 664–669, 2003.

[12] J. Schumann, S. Orgül, K. Gugleta, B. Dubler, and J. Flammer, "Interocular difference in progression of glaucoma correlates with interocular differences in retrobulbar circulation," *American Journal of Ophthalmology*, vol. 129, no. 6, pp. 728–733, 2000.

[13] Y. Yamazaki and S. M. Drance, "The relationship between progression of visual field defects and retrobulbar circulation in patients with glaucoma," *American Journal of Ophthalmology*, vol. 124, no. 3, pp. 287–295, 1997.

[14] X. Xu, "Acupuncture in an outpatient clinic in China: a comparison with the use of acupuncture in North America," *Southern Medical Journal*, vol. 94, no. 1-10, pp. 813–816, 2001.

[15] V. Napadow and T. J. Kaptchuk, "Patient characteristics for outpatient acupuncture in Beijing, China," *Journal of Alternative and Complementary Medicine*, vol. 10, no. 3, pp. 565–572, 2004.

[16] C. M. Witt, S. Jena, B. Brinkhaus, B. Liecker, K. Wegscheider, and S. N. Willich, "Acupuncture for patients with chronic neck pain," *Pain*, vol. 125, no. 1-2, pp. 98–106, 2006.

[17] B. Brinkhaus, C. M. Witt, S. Jena et al., "Acupuncture in patients with chronic low back pain: a randomized controlled trial," *Archives of Internal Medicine*, vol. 166, no. 4, pp. 450–457, 2006.

[18] D. Melchart, A. Streng, A. Hoppe et al., "Acupuncture in patients with tension-type headache: randomised controlled trial," *British Medical Journal*, vol. 331, no. 7513, pp. 376–379, 2005.

[19] C. Witt, B. Brinkhaus, S. Jena et al., "Acupuncture in patients with osteoarthritis of the knee: a randomised trial," *The Lancet*, vol. 366, no. 9480, pp. 136–143, 2005.

[20] K. Linde, A. Streng, S. Jürgens et al., "Acupuncture for patients with migraine: a randomized controlled trial," *Journal of the American Medical Association*, vol. 293, no. 17, pp. 2118–2125, 2005.

[21] *Diseases of Eyes, Ears, Nose and Throat*, vol. 681, Eastland Press, Seattle, Wash, USA, 1981.

[22] M. Kurusu, K. Watanabe, T. Nakazawa et al., "Acupuncture For Patients With Glaucoma," *Explore*, vol. 1, no. 5, pp. 372–376, 2005.

[23] S. Naruse, K. Mori, M. Kurihara et al., "Chorioretinal blood flow changes following acupuncture between thumb and forefinger," *Journal of Japanese Ophthalmological Society*, vol. 104, no. 10, pp. 717–723, 2000.

[24] M. Shimura, S. Uchida, A. Suzuki, K. Nakajima, and Y. Aikawa, "Reflex choroidal blood flow responses of the eyeball following somatic sensory stimulation in rats," *Autonomic Neuroscience*, vol. 97, no. 1, pp. 35–41, 2002.

[25] J. J. Steinle, D. Krizsan-Agbas, and P. G. Smith, "Regional regulation of choroidal blood flow by autonomic innervation in the rat," *American Journal of Physiology*, vol. 279, no. 1, pp. R202–R209, 2000.

[26] S. Takayama, T. Seki, N. Sugita et al., "Radial artery hemodynamic changes related to acupuncture," *Explore*, vol. 6, no. 2, pp. 100–105, 2010.

[27] S. Takayama, T. Seki, M. Watanabe et al., "Changes of blood flow volume in the superior mesenteric artery and brachial artery with abdominal thermal stimulation," *Evidence-Based Complementary and Alternative Medicine*, vol. 17, pp. 1–9, 2009.

[28] S. Takayama, T. Seki, M. Watanabe et al., "The herbal medicine Daikenchuto increases blood flow in the superior mesenteric artery," *Tohoku Journal of Experimental Medicine*, vol. 219, no. 4, pp. 319–330, 2009.

[29] S. Takayama, T. Seki, M. Watanabe et al., "The effect of warming of the abdomen and of herbal medicine on superior mesenteric artery blood flow—a pilot study," *Forschende Komplementarmedizin*, vol. 17, no. 4, pp. 195–201, 2010.

[30] S. Takayama, T. Seki, M. Watanabe et al., "Brief effect of acupuncture on the peripheral arterial system of the upper limb and systemic hemodynamics in humans," *Journal of Alternative and Complementary Medicine*, vol. 16, no. 7, pp. 707–713, 2010.

[31] E. T. Matthiessen, O. Zeitz, G. Richard, and M. Klemm, "Reproducibility of blood flow velocity measurements using colour decoded Doppler imaging," *Eye*, vol. 18, no. 4, pp. 400–405, 2004.

[32] S. S. Hayreh and R. Dass, "The ophthalmic artery II: intra orbital course," *The British Journal of Ophthalmology*, vol. 46, no. 3, pp. 165–185, 1962.

[33] A. K. Wiencke, H. Nilsson, P. J. Nielsen, and N. C. B. Nyborg, "Nonadrenergic noncholinergic vasodilation in bovine ciliary artery involves CGRP and neurogenic nitric oxide," *Investigative Ophthalmology and Visual Science*, vol. 35, no. 8, pp. 3268–3277, 1994.

[34] M. Shimura, S. Uchida, A. Suzuki, K. Nakajima, and Y. Aikawa, "Reflex choroidal blood flow responses of the eyeball following somatic sensory stimulation in rats," *Autonomic Neuroscience*, vol. 97, no. 1, pp. 35–41, 2002.

[35] D. Gherghel, S. Orgül, K. Gugleta, M. Gekkieva, and J. Flammer, "Relationship between ocular perfusion pressure and retrobulbar blood flow in patients with glaucoma with progressive damage," *American Journal of Ophthalmology*, vol. 130, no. 5, pp. 597–605, 2000.

[36] O. Zeitz, P. Galambos, L. Wagenfeld et al., "Glaucoma progression is associated with decreased blood flow velocities in the short posterior ciliary artery," *British Journal of Ophthalmology*, vol. 90, no. 10, pp. 1245–1248, 2006.

[37] F. Galassi, A. Sodi, F. Ucci, G. Renieri, B. Pieri, and M. Baccini, "Ocular hemodynamics and glaucoma prognosis: a color Doppler imaging study," *Archives of Ophthalmology*, vol. 121, no. 12, pp. 1711–1715, 2003.

[38] A. Martínez and M. Sánchez, "Predictive value of colour Doppler imaging in a prospective study of visual field progression in primary open-angle glaucoma," *Acta Ophthalmologica Scandinavica*, vol. 83, no. 6, pp. 716–722, 2005.

Clinical Ophthalmology

Dovepress
open access to scientific and medical research

Open Access Full Text Article

CASE REPORT

Observation of posterior corneal vesicles with in vivo confocal microscopy and anterior segment OCT

Ryou Watanabe
Toru Nakazawa
Nobuo Fuse

Department of Ophthalmology, Tohoku University Graduate School of Medicine, Sendai, Japan

Abstract: The histopathology of posterior corneal vesicles (PCV) has not yet been revealed. A 15-year-old girl, who was diagnosed by slit-lamp microscopy as PCV, was examined using specular microscopy, in vivo confocal microscopy, and anterior segment OCT (optical coherence tomography). Anterior segment OCT showed that the thickness of both corneas was within normal limits. At the same time, in vivo confocal microscopy revealed endothelial cells in the rounded dark areas, acellular hyporeflective layers on the Descemet's membrane, and hyperreflective linear lesions. These findings were not reported previously by slit-lamp and specular microscopy. The abnormal findings only existed at the Descemet's membrane and corneal endothelial layer. Previous reports dealing with posterior polymorphous dystrophy (PPMD) examined using in vivo confocal microscopy reported almost the same findings, suggesting that PCV and PPMD may be the same at the microstructural level.

Keywords: cornea, Descemet's membrane, imaging

Introduction

In 1924, Schnyder noted unilateral posterior vesicular lesions of the cornea as posterior herpes of the cornea.[1] However, in 1981, Pardos proposed a new concept of band-shaped structures at the level of the corneal posterior surface.[2] These were called posterior corneal vesicles (PCV) and were different from posterior herpes of the cornea as previously described. PCV is an uncommon, frequently asymptomatic, unilateral, noninherited disorder, which affects the corneal endothelium and Descemet's membrane. The lesions show horizontally parallel vesicles which contain small, numerous, roundish vacuoles at the posterior surface of the cornea.[2]

PCV has been previously diagnosed and reported by specular microscopy.[2,3] However, the histopathology of PCV remains unknown. The condition of PCV is stable,[2] and the corneal transplantation for PCV was not required and the pathological analysis for PCV was not performed. Here, in order to clarify the microstructure of PCV, we performed the imaging of PCV by in vivo confocal microscopy (Heidelberg Retina Tomograph II, Rostock Cornea Module [HRTII-RCM]; Heidelberg Engineering, Dossenheim, Germany) and anterior OCT (Visante™OCT; Carl Zeiss Meditec, Dublin, CA).

Case

A 15-year-old girl was referred to the Tohoku University General Hospital because of a suspicion of corneal dystrophy. On the right eye, slit-lamp examination revealed a horizontal band-shaped structure which contained small vesicles (Figure 1A, C).

Correspondence: Ryou Watanabe
Department of Ophthalmology, Tohoku University Graduate School of Medicine, 1-1 Seiryo-machi, Aoba-ku, Sendai, Miyagi 980-8574, Japan
Tel +81 22 717 7294
Fax +81 22 717 7298
Email ryo-w@oph.med.tohoku.ac.jp

submit your manuscript | www.dovepress.com
Dovepress
DOI: 10.2147/OPTH.S14550

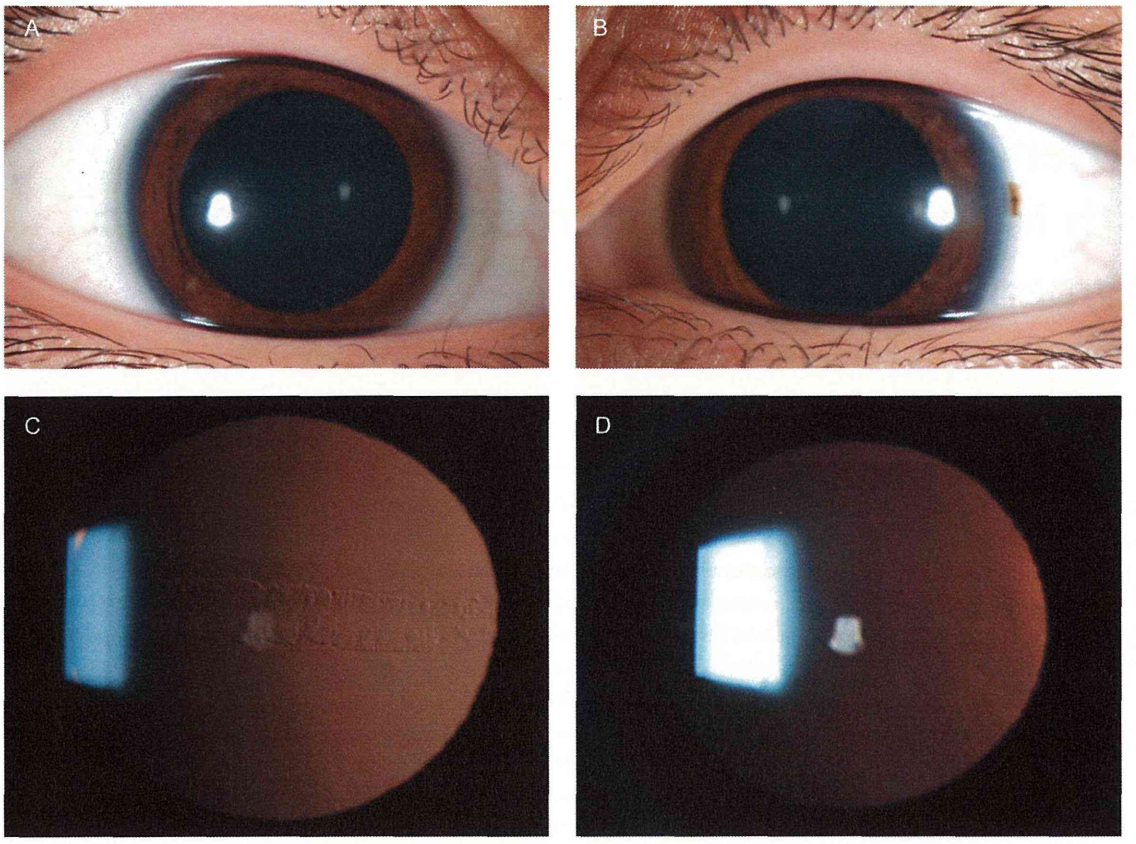

Figure 1 Observation using slit-lamp microscope. **A**) and **C**) affected eye. **B**) and **D**) normal eye.

The left eye was entirely normal (Figure 1B, D). Her mother's cornea had no abnormal findings. Specular microscope (Konan Noncon Specular microscope SP9000; Konan Medical, Inc., Hyogo, Japan) showed that the density of the corneal endothelium and the coefficient of variation were 1331, 1060, 1275 cells/mm^2 and 0.36, 0.67, 0.35 at the superior, middle, inferior section, respectively. At the middle area, the shape of the cell was irregular and some parts contained dark areas and bright spots inside the endothelium. In contrast, in the left eye, the density of the central corneal endothelium and coefficient of variation were 2941 cells/mm^2 and 0.33, and there were no abnormal findings. The patient was diagnosed as PCV. HRTII-RCM revealed that three different layers were clearly separated in the epithelial layer (superficial, wing, and basal cell layer) on the right eye and suggested that the patient had well-differentiated epithelial cells. In the subbasal nerve plexus layer, the number, bifurcation, and thickness of the nerves showed similar appearance (Figure 2A) to the left eye (Figure 2B), and no inflammatory cells were detected. In the substrate layer, we detected the normal number of keratocytes and neither Langerhans cells nor round leukocytes were detected, suggesting no inflammatory response in the stromal layer. Furthermore, close to the Descemet's membrane, the cell appearance and the number of the posterior stromal cells look normal (Figure 2C, D). In the Descemet's membrane layer, an acellular hyporeflective layer (Figure 2E, black arrows) and a hyperreflective linear lesion (Figure 2E, white arrows) were clearly detected (Figure 2E) because of winding the Descemet's membrane. In the endothelial layer, the various sizes of endothelial cells were observed on the vesicle area (Figure 2F, white arrows). In some endothelial cells, bright deposits of endothelial cells were observed (Figure 2F, black arrow). The rounded dark areas in the endothelial layer, which were also detected by specular microscopy, were observed more clearly by HRTII-RCM. Inside the dark area, probably protruded hypertrophy of Descemet's membrane, the monolayer of endothelial cells was observed (Figure 2G, white arrow). The left cornea showed that the margins of the endothelial cells were clear, the shapes of the cells stayed hexagonal, and the sizes of the cells were generally consistent (Figure 3A, B). All images

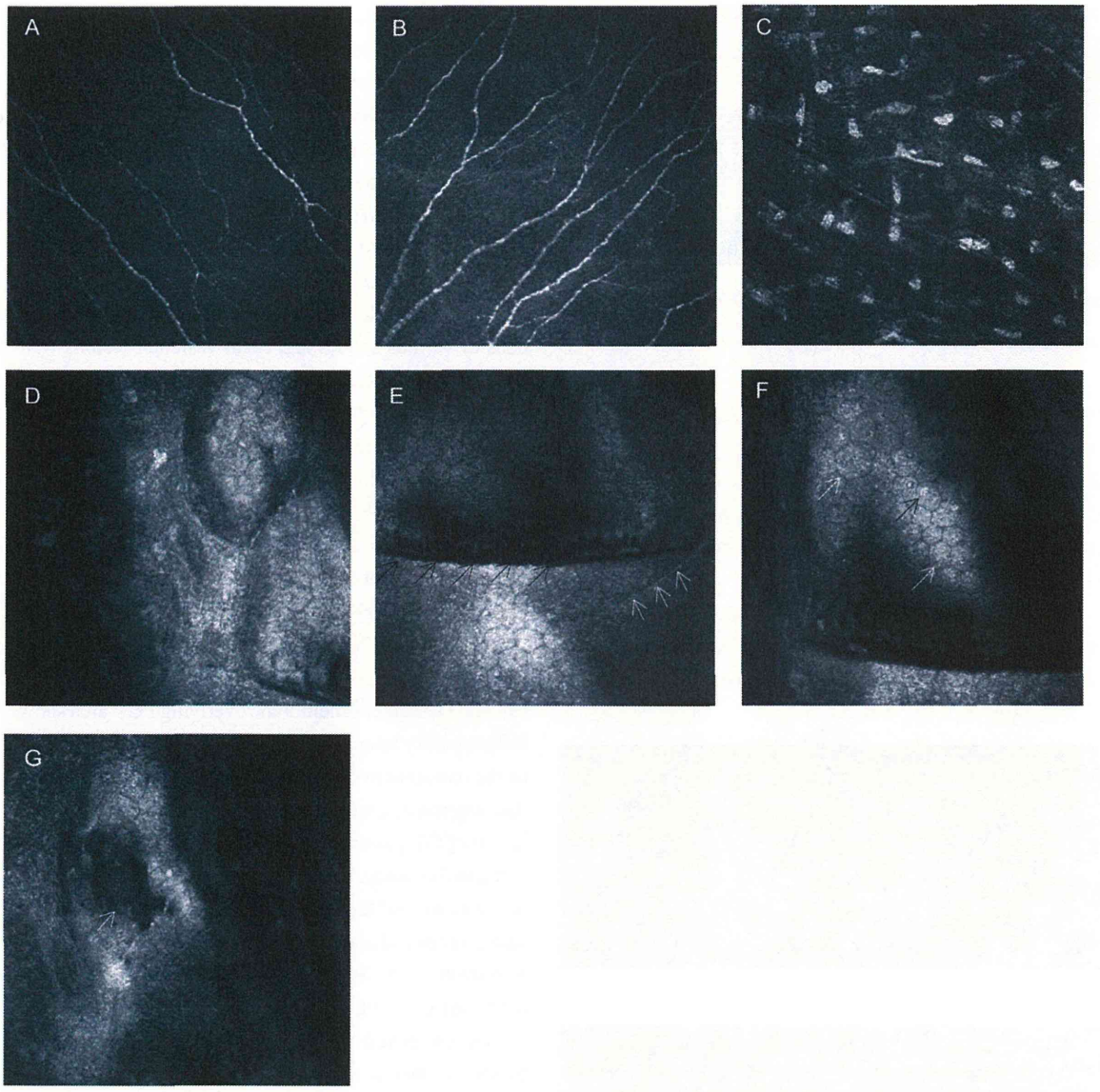

Figure 2 In vivo confocal microscopy showed that at the subbasal nerve plexus layer, number and thickness of the nerve were not different between **A**) right eye and **B**) left eye. **C**) The number of the keratocytes was normal at posterior stroma (524 μm). **D**) Next to the corneal endothelial cell, keratocyte of the posterior stroma was not hyperreflective (the picture was captured from oblique) (523 μm). **E**) An acellular hyporeflective layer (black arrows) and a hyperreflective linear lesion (white arrows) were seen (526 μm). **F**) Endothelial cells of various shapes (white arrows) (526 μm) and hyperreflective nuclear of the corneal endothelial cells (black arrow) (518 μm) were observed. **G**) Endothelial cells in the rounded dark area (547 μm).

of the Descemet's membrane and endothelial layer were captured at the center of the cornea.

On the right eye, anterior OCT revealed that the edge of vesicles on the endothelial layer was prominent toward the anterior chamber (Figure 4A, white arrows), and the lesions of prominent edge were also recognized by slit-lamp examinations (Figure 4B, white arrows). The central corneal thickness of the right and left eye was 572.6 ± 3.1 and 552.0 ± 8.2 μm, respectively. In both the cases, thickness was almost similar and within normal limits.

Discussion

PCV is very similar to posterior polymorphous dystrophy (PPMD) and it is difficult to differentiate these diseases using slit-lamp microscope and specular microscope. However, PCV is affected unilaterally and is a noninherited disease, enabling the diagnosis of PCV in this case. Differential diagnoses of PCV are listed as corneal guttata, congenital glaucoma, and forceps injury during the delivery. In this case, there were no characteristic findings of corneal guttata, which are titian-colored deposits at the central cornea, and

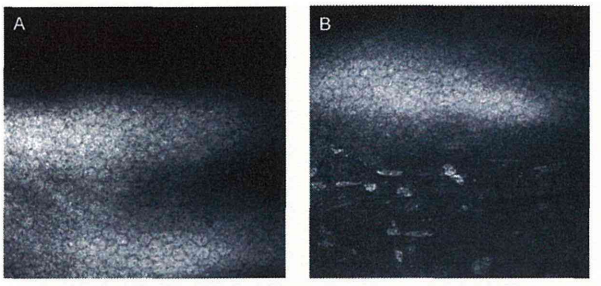

Figure 3 A) In vivo confocal microscopy showed that the left corneal endothelial cell showed the normal appearance. **B**) The image was captured obliquely and showed no abnormality of keratocytes in the adjacent corneal stroma to the endothelium.

brown deposits, which cause the 'beaten-metal appearance' at the posterior corneal surface. Delivery with forceps was ruled out due to no abnormality on the corneal surface. PCV is a unidentified virus-like structure in the place of the herpes cornea posterior. Therefore, the diagnosis of PCV was straightforward.

As far as we know, this is the first report describing the details of the in vivo microstructures of PCV using in vivo confocal microscopy. HRTII-RCM revealed endothelial cells in the rounded dark areas, acellular hyporeflective layers, and hyperreflective linear lesions. Usually, Descemet's membrane is not visualized in normal subjects. The winding of the Descemet's membrane is not detected in the normal subjects usually. And this winding of Descemet's membrane is one of the characteristic findings with this disease. So in this report, we can detect clearer thickened membranes which were not reported previously using slit-lamp and specular microscopes.[2,3] On the other hand, endothelial cells which contained bright deposits at affected areas as well as endothelial cells of various shapes and focal vesicular lesions were also observed. These characteristic appearances were observed in the previous reports with specular microscope.[2] Furthermore, HRTII-RCM can reveal additional information because HRTII-RCM enables us to obtain images of the various corneal layers easily using confocal techniques. We routinely get images including superficial, wing, and basal cell layer of epithelium, subbasal nerve plexus layer, Bowman's membrane, stromal layer (anterior [100–200 μm], middle [250–350 μm], posterior [400–500 μm]), Descemet's membrane layer, and endothelial layer. We found that the lesions close to the corneal endothelial cell and Descemet's membrane overlying PCV area showed no inflammatory responses like the proliferation of keratocytes, or the recruitment of Langerhans cells and leukocytes. These data suggest that the epithelium and stroma overlying the PCV lesion of this patient were within normal limits. On the other hand, in this study, we recognized that Descemet's membrane was winding and the monolayer endothelial cells were detected inside the rounded dark areas. These findings suggest that the hypertrophy of Descemet's membrane was involved in the pathogenesis of PCV.

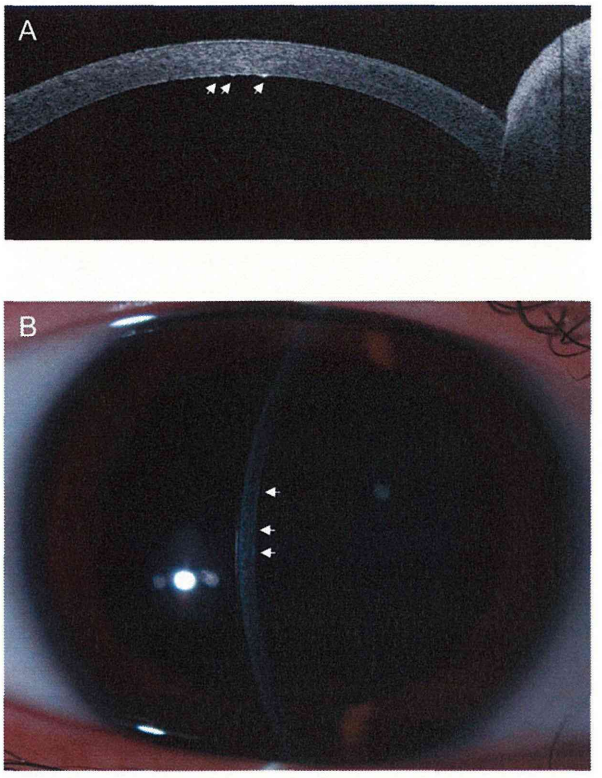

Figure 4 A) Protuberance (white arrows) toward the anterior chamber was observed with anterior OCT on right eye. **B**) Slit-lamp microscope findings. White arrows indicated that the protuberance was located at the same places when compared with the OCT observation.

We compared the findings for PCV with PPMD using in vivo confocal microscopy. Both findings were similar. There have been some papers describing PPMD using in vivo confocal microscopy.[4–7] HRTII-RCM showed that in this case abnormal findings were detected at only corneal endothelial cells and Descemet's membrane. A comparison with previous reports shows that some findings were consistent with PPMD: acellular hyporeflective layers, hyperreflective linear lesions, endothelial cells containing bright nuclei, varied cell shapes, endothelial cells inside the rounded dark areas, focal vesicular lesions, and hyperreflective areas around the rounded dark areas. Other findings were different: the increased number and density of the posterior keratocytes in one case among six cases,[4] the thickened nerve at the Bowman's membrane,[5] and needle-like lesion in the stroma with few keratocytes.[7] However, these findings may suggest that one case with PPMD associated with inflammations.

In the right cornea of this case, the density of the corneal endothelial cells had already decreased to ~1000 cells/mm^2 at the center of the cornea. Generally, the density of corneal endothelial cells is more than 3000 cells/mm^2 for patients of the same age.[8] Using anterior OCT, we found that the thickness of the right cornea was almost the same as the normal left cornea, implying that the function of the Na^-/K^+-ATPase pump, and the barrier of endothelial cell was being kept at a normal range and maintaining the thickness of the cornea. However, endothelial cells never regenerate and their number decreases with age. The age of the patient is 15 and she needs long-term observation, especially concerning the density of her endothelium. Usually, PCV does not affect visual acuity. Up to now, the rate of decrease in cell density of a normal endothelium is ~0.6% per year.[8] We need to pay attention in the follow-up examination not only to the natural course of the decreasing cell density in the endothelium but also to hypoxic and mechanical stress to endothelial cells, which occurs as a result of wearing contact lens and eye surgery to prevent the bullous keratopathy.

Using the HRTII-RCM, for the first time, it was possible to observe endothelial cells in rounded dark areas, hyperreflective linear lesions, and acellular hyporeflective layers. There was also no detected increase of density and brightness of keratocytes; in addition the nerve plexus showed a normal shape. Anterior OCT revealed protuberances toward the anterior chamber and no difference in the thickness of either cornea. In this case, we should observe the density of the corneal endothelial cells carefully.

Disclosure

The authors report no conflicts of interest in this work.

References

1. Schnyder W. Herpetiforme Erkrankung der Hornhautrückfläche [Herpes corneae posterior]. *Klin Mbl Augenheilk*. 1924;73:385–390.
2. Pardos GJ, Krachmer JH, Mannis MJ. Posterior corneal vesicles. *Arch Ophthalmol*. 1981;99(9):1573–1577.
3. Harada T, Tanaka H, Ikema T, Asakura K, Miura M, Ozeki Y. Specular microscopic observation of posterior corneal vesicles. *Ophthalmologica*. 1990;201(3):122–127.
4. Patel DV, Grupcheva CN, McGhee CN. In vivo confocal microscopy of posterior polymorphous dystrophy. *Cornea*. 2005;24(5):550–554.
5. Grupcheva CN, Chew GS, Edwards M, Craig JP, McGhee CN. Imaging posterior polymorphous corneal dystrophy by in vivo confocal microscopy. *Clin Experiment Ophthalmol*. 2001;29(4):256–259.
6. Cheng LL, Young AL, Wong AK, Law RW, Lam DS. Confocal microscopy of posterior polymorphous endothelial dystrophy. *Cornea*. 2005;24(5):599–602.
7. Babu K, Murthy KR. In vivo confocal microscopy in different types of posterior polymorphous dystrophy. *Indian J Ophthalmol*. 2007;55(5):376–378.
8. Bourne WM, Nelson LR, Hodge DO. Central corneal endothelial cell changes over a ten-year period. *Invest Ophthalmol Vis Sci*. 1997;38(3):779–782.

Hindawi Publishing Corporation
Journal of Ophthalmology
Volume 2011, Article ID 940323, 4 pages
doi:10.1155/2011/940323

Case Report

Successful Removal of Large Intraocular Foreign Body by 25-Gauge Microincision Vitrectomy Surgery

Hiroshi Kunikata,[1] Megumi Uematsu,[1] Toru Nakazawa,[2] and Nobuo Fuse[1]

[1] *Department of Ophthalmology and Visual Science, Tohoku University Graduate School of Medicine, 1-1 Seiryo-machi, Aoba-ku, Sendai 980-8574, Japan*
[2] *Division of Visual Advanced Medicine, Tohoku University Graduate School of Medicine, Sendai 980-8574, Japan*

Correspondence should be addressed to Hiroshi Kunikata, kunikata@oph.med.tohoku.ac.jp

Received 30 October 2010; Accepted 23 February 2011

Academic Editor: Edward Manche

We describe a new technique for removing a large intraocular foreign body by 25-gauge microincision vitrectomy surgery (25G-MIVS). Noncomparative interventional case series were performed at a single centre. Two patients with a long smooth intraocular vitreal foreign body underwent phacoemulsification and aspiration, intraocular lens implantation, 25G-MIVS, and extraction of the foreign body. The foreign body was removed through a posterior capsulorhexis, anterior continuous curvilinear capsulorhexis, and a corneal incision. In both cases, the foreign body was safely removed through the corneal incision, and IOL was implanted and well positioned. The surgical incision did not require suturing. No postoperative complications associated with this technique were found. The corneal endothelial cell density was maintained over 2000 cells/mm^2 in both cases during recent follow-up examinations. Our findings indicate that 25G-MIVS with this technique can be used to extract a long slender smooth foreign body. It is safe, without complications, and can be performed without enlarging the 25-gauge sclerotomy.

1. Introduction

The removal of an intraocular foreign body is difficult, and less invasive techniques that lead to good postoperative vision from the early stage are being investigated. If a large foreign body is extracted from the eye, an enlargement of the sclerotomy is needed, and intraoperative suturing is required. The suturing usually leads to corneal astigmatism.

25-gauge microincision vitrectomy surgery (25G-MIVS) was first reported in 2002, and this technique is commonly used worldwide for various retinal diseases including rhegmatogenous retinal detachments [1–4]. The increase in the use of MIVS has been enhanced by studies that demonstrated significant reductions in postoperative astigmatism, conjunctival injection, pain, and discomfort [5–7]. However, the use of 25G-MIVS for the removal of a foreign body without an enlargement of the sclerotomy had not been reported [8, 9].

The purpose of this study was to determine whether 25G-MIVS can be used to remove an intraocular foreign body without suturing.

2. Technique

Case 1. A 31-year-old man presented 4 days after a corneal laceration in the temporal area of the right eye (Figure 1(a)). His best-corrected visual acuity (BCVA) was 6/20, and the intraocular pressure was normal. The corneal wound was self-sealed without any leakage, but a small penetrating wound was seen in his right iris at the 9 o'clock position. Slit-lamp examination showed a posterior subcapsular cataract at the same position. Fundus examination showed vitreous haemorrhage, and computed tomography showed a metallic foreign body in the vitreous (Figure 1(b)).

The foreign body was a straight metallic nail without a head that was 1.0 mm in diameter and 7.0 mm long

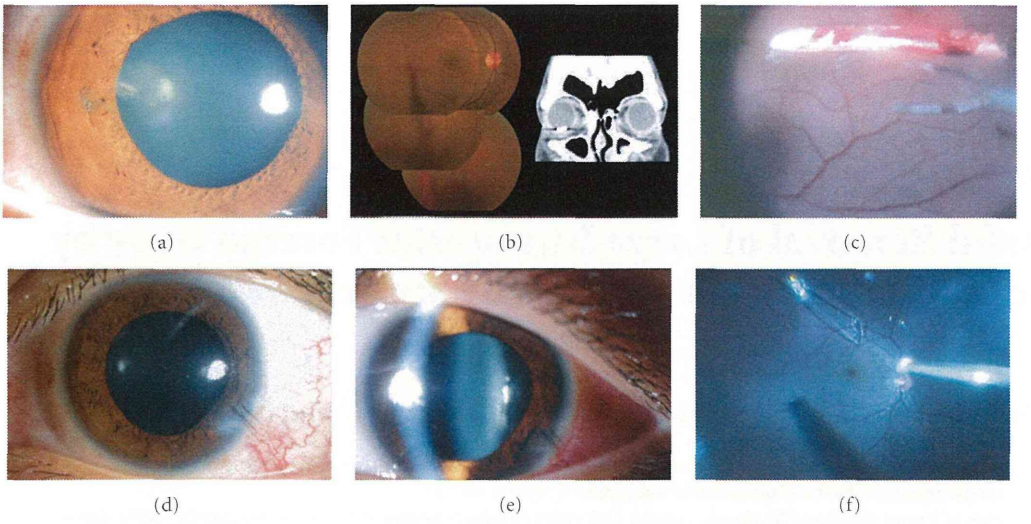

FIGURE 1: Preoperative slit-lamp photographs, preoperative fundus photograph, preoperative computed tomographic image, and intraoperative photographs of intraocular foreign body (Case 1; (a, b, c), Case 2; (d, e, f)). (a) Preoperative slit-lamp photograph shows a slight penetrating wound in the iris and lens at the 9 o'clock position and a posterior subcapsular cataract at the same position. (b) Fundus photograph showing vitreous haemorrhage and retinal tear with subretinal haemorrhage located on the temporal side of the macula. Computed tomographic image showing a large foreign body. (c) Intraoperative fundus showing a large metallic intraocular foreign body anterior to the retina. (d) External photograph showing the penetrating wound at the 4 o'clock position and the corneal wound was closed by corneal sutures during the initial surgery. (e) Slit-lamp photograph showing that the posterior subcapsular cataract has progressed. (f) Intraoperative fundus photograph showing large glass intraocular foreign body anterior to the retina.

(Figure 1(c)). We performed phacoemulsification and aspiration (PEA) through a 2.4 mm corneal incision, 25G-MIVS, and extracted the foreign body. First, we picked up the foreign body off of the retina with forceps and moved it into the vitreous cavity. Then, it was moved into the anterior chamber through a posterior capsulorhexis and an anterior continuous curvilinear capsulorhexis, and we grasped the foreign body with another forceps and removed the foreign body through the corneal wound which was used for PEA. Thus, the foreign body was extracted through a posterior capsulorhexis, an anterior continuous curvilinear capsulorhexis, and the corneal incision (triple C-through technique; Figures 2(a) and 2(b)). In addition, endophotocoagulation was performed on a retinal tear and on the area surrounding a subretinal haemorrhage located on the temporal side of the macula. An intraocular lens (IOL) was implanted in the capsular bag. All wounds including the incision for the cataract and vitreous surgeries did not require any suturing, and the IOL was well positioned (Figure 2(c)).

One month after the surgery, the BCVA was 20/20, and this BCVA was maintained for 32 months. No postoperative complications except a small epiretinal membrane developed during the 32 months of followup. The corneal endothelial cell density at baseline and at 32 months was 2834 and 2288 cells/mm^2, respectively.

Case 2. A 21-year-old man presented with a 7-day-old corneal laceration at the 4 o'clock position of the left eye (Figure 1(d)). The wound was closed by the initial surgery, and there was a trace of a penetrating wound in the corresponding iris at same position. Slit-lamp examination showed a posterior subcapsular cataract (Figure 1(e)). Indirect ophthalmoscopy showed that the vitreous was clear, but there was a large glass-like object in the vitreous free from the retina (Figure 1(f)). The foreign body was a piece of glass that was 2.0 mm wide and 8.0 mm long. The retina around the foreign body was not inflamed. The BCVA was 20/20 in his left eye, and the intraocular pressure was normal.

We performed PEA through a 2.4 mm corneal incision, 25G-MIVS, extraction of the foreign body, and implantation of an IOL in the sulcus. Before grasping the foreign body with 25-gauge forceps, perfluorocarbon liquid (PFCL) was used to float the foreign body above the retina and macula. The floating foreign body was located at the margin of the PFCL because of its buoyancy, gravity, and PFCL's surface tensity, and we grasped the foreign body with forceps and removed it as in Case 1. Thus, the foreign body was extracted through a posterior capsulorhexis, an anterior continuous curvilinear capsulorhexis, and the corneal incision (triple C-through technique; Figures 2(d) and 2(e)). The 2.4 mm corneal incision was slightly enlarged to 3 mm to extract the foreign body safely. All of the surgical wounds including that for the cataract surgery required no suturing (Figure 2(f)).

One month after the surgery, the BCVA was 20/20, and this BCVA was maintained for 6 months, and no complications developed during the six-month followup. The corneal endothelial cell density at baseline and at 6 months was 2884 and 3021 cells/mm^2, respectively.

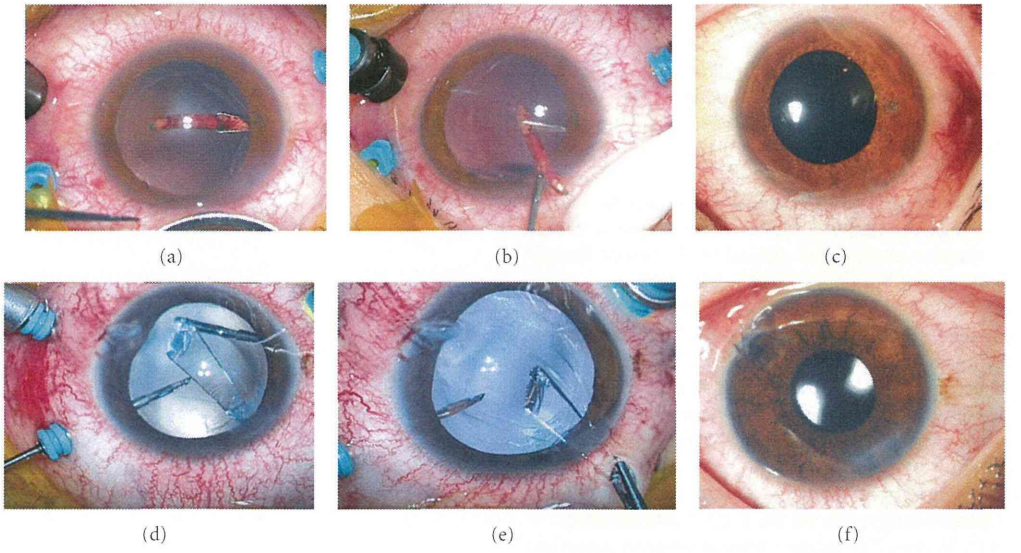

FIGURE 2: Intraoperative photographs and postoperative slit-lamp photographs of Case 1 (a, b, c) and Case 2 (d, e, f). (a) and (b) Metallic foreign body extracted through an anterior and posterior capsulorhexis, and corneal incision (triple C-through technique). (c) Slit-lamp photograph (inverted image as seen by the surgeon) 1 day postoperatively showing no need of suturing, no subconjunctival haemorrhage, and well-positioned intraocular lens. (d) and (e) Glass foreign body extracted through an anterior and posterior capsulorhexis, and corneal incision (triple C-through technique). (f) Slit-lamp photograph (inverted image as seen by the surgeon) 1 day postoperatively showing no need of suturing, except the original penetration wound, no subconjunctival haemorrhage and well-positioned intraocular lens.

3. Discussion

The removal of a foreign body usually requires a relatively large sclerotomy, and closing the sclerotomy with sutures often leads to postoperative corneal astigmatism. In addition, extracting a foreign body through the sclerotomy can damage the ciliary body and peripheral retina because it is difficult to see the foreign body when it is being extracted. Thus, we believe that extracting a foreign body through a small corneal wound that does not require suturing is a safer way to obtain good vision postoperatively.

The extraction of a foreign body through a 6 mm sclerocorneal tunnel using 20-gauge conventional vitrectomy instruments was recently reported [8]; however, the scleral incision required suturing. The use of 25G-MIVS to remove foreign body has also been reported, although an enlargement of the sclerotomy was required in all cases [9]. We combined posterior capsulorhexis with microincision cataract surgery (corneal incision 2.4 mm) and vitreous surgery (25G-MIVS) as a safe method of extracting a foreign body without complications and not requiring suturing.

Our study has several weaknesses, including its retrospective nature, only two cases, and short follow-up periods. However, we had very good results, and we recommend that a soft shell be used to protect the corneal endothelial surface and care be taken to keep the foreign body from touching the corneal endothelial surface. PFCL also should be used to protect the posterior part of retina for an accidental falling of the foreign body during this procedure. This technique of triple C-through technique is probably best suited to a long slender smooth foreign body and should not be used for larger foreign bodies of odd shape.

In conclusion, under favorable conditions of intraocular foreign bodies, we recommend 25G-MIVS to remove foreign bodies safely without suturing. Further investigations including evaluation of the postoperative visual quality and complications are needed to determine efficacy of this procedure.

Disclosure

This paper was presented partially at the Annual Meeting of the 31th Japanese Society of Ophthalmic Surgeons, Yokohama, February 2008.

References

[1] G. Y. Fujii, E. De Juan Jr., M. S. Humayun et al., "Initial experience using the transconjunctival sutureless vitrectomy system for vitreoretinal surgery," *Ophthalmology*, vol. 109, no. 10, pp. 1814–1820, 2002.

[2] G. Y. Fujii, E. De Juan Jr., M. S. Humayun et al., "A new 25-gauge instrument system for transconjunctival sutureless vitrectomy surgery," *Ophthalmology*, vol. 109, no. 10, pp. 1807–1812, 2002.

[3] M. Mura, S. H. Tan, and M. D. De Smet, "Use of 25-gauge vitrectomy in the management of primary rhegmatogenous retinal detachment," *Retina*, vol. 29, no. 9, pp. 1299–1304, 2009.

[4] H. Kunikata and K. Nishida, "Visual outcome and complications of 25-gauge vitrectomy for rhegmatogenous retinal

detachment; 84 consecutive cases," *Eye*, vol. 24, no. 6, pp. 1071–1077, 2010.

[5] K. Kadonosono, T. Yamakawa, E. Uchio, Y. Yanagi, Y. Tamaki, and M. Araie, "Comparison of visual function after epiretinal membrane removal by 20-gauge and 25-gauge vitrectomy," *American Journal of Ophthalmology*, vol. 142, no. 3, pp. 513–515, 2006.

[6] L. Kellner, B. Wimpissinger, U. Stolba, W. Brannath, and S. Binder, "25-gauge vs 20-gauge system for pars plana vitrectomy: a prospective randomised clinical trial," *British Journal of Ophthalmology*, vol. 91, no. 7, pp. 945–948, 2007.

[7] C. W. Tsang, B. T. Cheung, R. F. Lam et al., "Primary 23-gauge transconjunctival sutureless vitrectomy for rhegmatogenous retinal detachment," *Retina*, vol. 28, no. 8, pp. 1075–1081, 2008.

[8] S. K. Mahapatra and N. G. Rao, "Visual outcome of pars plana vitrectomy with intraocular foreign body removal through sclerocorneal tunnel and sulcus-fixated intraocular lens implantation as a single procedure, in cases of metallic intraocular foreign body with traumatic cataract," *Indian Journal of Ophthalmology*, vol. 58, no. 2, pp. 115–118, 2010.

[9] S. Kiss and D. Vavvas, "25-gauge transconjunctival sutureless pars plana vitrectomy for the removal of retained lens fragments and intraocular foreign bodies," *Retina*, vol. 28, no. 9, pp. 1346–1351, 2008.

Journal of Neuroscience Research

Journal of Neuroscience Research 90:802–815 (2012)

Critical Role of Calpain in Axonal Damage-Induced Retinal Ganglion Cell Death

**Morin Ryu,[1] Masayuki Yasuda,[1] Dong Shi,[1,2] Ahmed Y. Shanab,[1] Ryo Watanabe,[1] Noriko Himori,[1] Kazuko Omodaka,[1] Yu Yokoyama,[1] Jiro Takano,[3] Takaomi Saido,[3] and Toru Nakazawa[1]*

[1]Department of Ophthalmology, Tohoku University Graduate School of Medicine, Miyagi, Japan
[2]Department of Ophthalmology, The Fourth Affiliated Hospital, China Medical University, Liaoning, China
[3]Laboratory for Proteolytic Neuroscience, RIKEN Brain Science Institute, Saitama, Japan

Calpain, an intracellular cysteine protease, has been widely reported to be involved in neuronal cell death. The purpose of this study is to investigate the role of calpain activation in axonal damage-induced retinal ganglion cell (RGC) death. Twelve-week-old male calpstatin (an endogenous calpain inhibitor) knockout mice (CAST KO) and wild-type (WT) mice were used in this study. Axonal damage was induced by optic nerve crush (NC) or tubulin destruction induced by leaving a gelatin sponge soaked with vinblastine (VB), a microtubule disassembly chemical, around the optic nerve. Calpain activation was assessed by immunoblot analysis, which indirectly quantified the cleaved α-fodrin, a substrate of calpain. RGCs were retrogradely labeled by injecting a fluorescent tracer, Fluoro-Gold (FG), and the retinas were harvested and flat-mounted retinas prepared. The densities of FG-labeled RGCs harvested from the WT and CAST KO groups were assessed and compared. Additionally, a calpain inhibitor (SNJ-1945, 100 mg/kg/day) was administered orally, and the density of surviving RGCs was compared with that of the vehicle control group. The mean density of surviving RGCs in the CAST KO group was significantly lower than that observed in the WT group, both in NC and in VB. The mean density of surviving RGCs in the SNJ-1945-treated group was significantly higher than that of the control group. The calpain inhibitor SNJ-1945 has a neuroprotective effect against axonal damage-induced RGC death. This pathway may be an important therapeutic target for preventing this axonal damage-induced RGC death, including glaucoma and diabetic optic neuropathy and other CNS diseases that share a common etiology.

Key words: calpastatin; axonal damage; glaucoma; SNJ1945; neuroprotection

Glaucoma affects 70 million people worldwide and is a secondary cause of blindness (Quigley, 1996; Resnikoff et al., 2004). Glaucoma is characterized by glaucomatous optic neuropathy (GON) and is associated with optic nerve fiber atrophy that results in progressive visual loss (Weinreb and Khaw, 2004). Although increased intraocular pressure (IOP) is widely recognized as a major risk factor for glaucoma, the pathogenesis of the disease remains unclear. Lowering IOP is currently the only standard treatment to prevent disease progression (Heijl et al., 2002), and different eye drops are used for the treatment of glaucoma in the clinic. However, some patients with significant IOP reduction still show disease progression (Anderson et al., 1998). Normal-tension glaucoma (NTG) is a major type of glaucoma (Iwase et al., 2004), particularly in Asia, with myopia and aging, in addition to high IOP, being major risk factors (Suzuki et al., 2006). Currently, the pathogenesis of retinal ganglion cell (RGC) death in patients with NTG has yet to be elucidated, even though RGCs are known to be particularly vulnerable (Levin, 2003). Neuroprotection against RGC death has been emphasized as an important goal in disease management (Levin, 2003), but this has yet to be achieved.

Calpains are a family of 14 calcium-regulated, intracellular cysteine proteases, which modulate cellular functions through a limited, specific proteolysis (Huang

Contract grant sponsor: Ministry of Education, Science and Technology of Japan; Contract grant number: 21659395 (to T.N.); Contract grant number: 22689045 (to T.N.); Contract grant sponsor: Uehara Memorial Research Foundation; Contract grant sponsor: Takeda Research Foundation; Contract grant sponsor: Imai Glaucoma Research Foundation; Contract grant sponsor: Japanese National Society for the Prevention of Blindness (to T.N.).

*Correspondence to: Toru Nakazawa, MD, PhD, Department of Ophthalmology, Tohoku University Graduate School of Medicine, 1-1 Seiryo, Aoba, Sendai, Miyagi, 980-8574 Japan.
E-mail: ntoru@oph.med.tohoku.ac.jp

Received 16 May 2011; Revised 22 August 2011; Accepted 30 August 2011

Published online 8 November 2011 in Wiley Online Library (wileyonlinelibrary.com). DOI: 10.1002/jnr.22800

and Wang, 2001). Calpain-1 (mu-calpain) and calpain-2 (m-calpain) are the two major typical calpain isoforms. In various pathological systemic diseases, including renal ischemic injury (Chatterjee et al., 2005) and intestinal ischemia (Marzocco et al., 2004), and in central nervous system (CNS), an overload of calcium ion (Ca^{2+}) influx in cytosol leads to cellular death (Camins et al., 2006). Calpains are members of the cysteine protease family activated by increased intracellular Ca^{2+} levels (Camins et al., 2006) raised locally through calcium channels, such as voltage-gated calcium channels, intracellular stores, and N-methyl-D-aspartate (NMDA) receptors. Activated calpains cleave several substrates, including α-spectrin (Nath et al., 1996), calcineurin (Wu et al., 2004), subunits of the NMDA receptor NR2A (Guttmann et al., 2002) and NR2B (Simpkins et al., 2003), NCAM (Sheppard et al., 1991), and p35 (Patrick et al., 1999). The cleavage effects of activated calpain lead to apoptotic cell death, and calpain signaling is involved in several pathological conditions (Bizat et al., 2003a,b; Chiu et al., 2005).

For the visual system, as a part of the CNS, calpain-dependent damage had been reported in many retinal disease (Azuma and Shearer, 2008). Our previous studies have demonstrated that calpain-dependent dephosphorylation of Akt plays a critical role in NMDA-induced retinal cell death in vivo (Nakazawa et al., 2005, 2009). Retinal excitotoxicity is involved in vessel occlusion (Matini et al., 1997), diabetic retinopathy (Ambati et al., 1997; Deng et al., 2000), and acute ocular hypertension (Lam et al., 1997). Therefore, the inhibition of the calpain pathway is thought to be therapeutic against various retinal diseases. Recently, calpain expression and activation have been shown in an experimental model of glaucoma (Huang et al., 2010; Qu et al., 2010) and RGC death in vitro (McKernan et al., 2007); however, the details of whether the ocular hypertension-induced calpain activation has a causative role in RGC death remain unknown. Insights into the mechanisms of axonal damage-induced RGC death are urgently needed to aid in the development of new neuroprotective treatment strategies for patients with glaucoma.

In this study, we developed a mouse model of axonal damage and investigated whether the calpain pathway had a causative role in axonal damage-induced RGC death. In addition, we examined whether the inhibition of calpain would be a useful drug target in the treatment of glaucoma.

MATERIALS AND METHODS

Animals

In total, 133 male wild-type mice (C57BL6, age 12 weeks, 23–27 g) and 87 calpastatin (CAST) KO mice (Higuchi et al., 2005; Takano et al., 2005; age 12 weeks, 25–30 g) were used. The surgical procedures were performed with animals under deep anesthesia with an intramuscular administration of a mixture of ketamine (100 mg/kg) and xylazine (9 mg/kg). All mice were euthanatized with an intraperitoneal injection of a lethal dose of pentobarbital.

All animals were maintained and handled in accordance with the principles presented in the guidelines for the use of animals in neuroscience research and the guidelines from the Declaration of Helsinki and the guiding principles in the care and use of animals. All experimental procedures described here were approved by the Ethics Committee for Animal Experiments at Tohoku University Graduate School of Medicine. All animals were treated according to the National Institutes of Health guidelines for the care and use of laboratory animals.

Drugs

For oral administration, calpain inhibitor powder (SNJ-1945, molecular weight 909; Senju Pharmaceutical Co.) was suspended in distilled water with 0.5% carboxymethyl cellulose (CMC) and orally administered (0.5 ml, 100 mg/kg) every day until sacrifice. CMC (0.5 ml) was given as a control. On the day of surgery, SNJ-1945 was administered orally 1 hr before the nerve crush procedure or vinblastine treatment. In vitro, SNJ-1945 was dissolved in dimethylsulfoxide (DMSO; 046-21981; Wako) and then further diluted (final concentration 4 and 40 μM, 0.1% of DMSO) in the culture medium Neurobasal-A (10888-022; Invitrogen, Carlsbad, CA). Brain-derived neurotrophic factor (BDNF; 450-02; Peprotech, Rocky Hill) was dissolved in phosphate-buffered saline (0.5 μg/μl) with 0.1% bovine serum albumin (BSA). Immediately following the nerve crush or vinblastine administration, a 2-μl solution of BDNF was injected into right vitreous of the mice. Tat-BH4 (197217; Bcl-xL BH44-23; EMD Chemicals, Gibbstown, NJ) was dissolved in 100% DMSO and diluted 10 times with saline to a final concentration 1 μg/μl. Thirty minutes before the nerve crush or vinblastine administration, 200 μl Tat-BH4 solution was administered intraperitoneally (20 mg/kg).

Surgery

The neuronal retrograde tracer Fluoro-Gold 2% (FG; Fluorochrome, LLC, Denver, CO) was prepared in saline, and 1,1′-dioctadecyl-3,3,3′,3′-tetramethylindocarbocyanine perchlorate 1% (Di-I, 468495; Sigma-Aldrich, St. Louis, MO) was prepared in DMSO. Seven days before the surgery, retrograde labeling was performed as described previously (Nakazawa et al., 2006, 2007b). Briefly, the animal was anesthetized and the skin over the cranium was incised to expose the scalp. A hole 1 mm in diameter was made on each side of the skull with a drill at 4 mm posterior to the bregma and 1 mm lateral to the midline. One microliter of 2% FG solution or 1% Di-I solution was slowly injected at a 2-mm depth from the surface of skull with a Hamilton syringe equipped with a 32-G needle. The overlying skin was sutured with 6-0 nylon, and antibiotic ointment was externally applied.

Seven days after retrograde labeling, optic nerve surgery was performed. After exposure of the optic nerve, the nerve was crushed with fine forceps for 10 sec and released. Blood circulation was confirmed to be normal, and antibiotic ointment was applied. For the vinblastine model, after blunt dis-

section of periocular connective tissue, the optic nerve was exposed. Vinblastine (1377; Sigma-Aldrich) was dissolved in saline at several concentrations: 0.1, 1, 3, and 10 mM. The gelatin sponge Spongel (rent to 2 mm^3; Yamanouchi, Japan) soaked in vinblastine solution was placed around the optic nerve. Blood circulation was confirmed to be normal, and antibiotic ointment was externally applied.

Retinal Flat Mount and RGC Counting

For the count of the RGCs surviving following the axonal (nerve crush or vinblastine treatment) damage, the retinas were harvested 3, 7, 10, 14, and 28 days after surgery for time-course analysis. For the vinblastine dose-dependent analysis and SNJ-1945 treatment, the retinas were harvested 7 days after the surgery. All retinas were flat mounted, and the density of RGCs was counted under a fluorescent microscope (Axiovert 200; Carl Zeiss, Oberkochen, Germany) as previously described (Nakazawa et al., 2006, 2007b). Briefly, retinas were fixed in 4% paraformaldehyde (PFA) for 2 hr. Then retinas were flat mounted onto glass slides, and RGCs labeled with FG or Di-I were counted in 12 distinct areas of 2.46×10^{-2} mm^2 each (three areas per retinal quadrant at one-sixth, one-half, and five-sixths of the retinal radius). The density of the RGCs was defined as an average value of the 12 fields. The counting was performed by three independent investigators in a masked fashion, and the data were averaged.

Primary Culture and βIII-Tubulin Positive Cells Counting

Primary culture of retinas was performed as previously described (Nakazawa et al., 2007a,b). Briefly, retinas were dissected and dissociated with a papain digestion solution for 15 min. The suspended retinal mixed cells were seeded (5,700 cells/mm^2) onto a CC2-coated chamber slide (154941; Thermo Fisher Scientific, Waltham, MA) and kept in Neurobasal-A medium (10888-022; Invitrogen) with 5% B27 supplement, 0.5 mM L-glutamine (25030-149; Invitrogen), 0.25 mg/ml gentamicin (G1397; Sigma-Aldrich), and 5 μg/ml insulin (I6634; Sigma-Aldrich), with or without SNJ-1945 (4 and 40 μM). The cells were incubated for 24 hr before being fixed for immunocytochemistry.

Five images were captured (450 × 330 mm) randomly from each well of the chamber slide. The βIII-tubulin$^+$ cells were counted by three independent investigators in a masked fashion, and DAPI$^+$ cells were counted by WinRoof software (version 5.8.1; Mitani Co.). There were four wells for each condition, and the average percentage of βIII-tubulin$^+$ cells/DAPI$^+$ cells was calculated for further analysis.

Immunohistochemistry and Immunocytochemistry

Immunohistochemistry (IHC) and immunocytochemistry (ICC) were performed as previously reported (Nakazawa et al., 2007a, 2009). For IHC, surgically removed eyes still attached to the optic nerve were fixed with 4% PFA overnight at 4°C and then cryoprotected with PBS with 20% sucrose. Cryosections (thickness 10 μm) were mounted on the slides and incubated with blocking buffer (10% goat serum, 0.5% gelatin, 3% BSA and 0.2% Tween 20 in PBS). Next, they were incubated with mouse monoclonal antibodies against neurofilament (RT-97; 1:200; ab17126; Abcam, Cambridge, United Kingdom) for 2 hr at room temperature. The sections were washed three times with PBST (PBS containing 0.2% Tween 20) and then incubated with an Alexa 488 secondary antibody (1:200; A11029; Invitrogen) for 1 hr. The slides were washed three times and mounted with Vectashield mounting medium (H1000; Vector, Burlingame, CA).

For ICC, the retinal mixed-culture cells seeded on the chamber slide were fixed with 4% PFA for 10 min at room temperature. After blocking as described above, they were incubated with monoclonal anti-βIII-tubulin antibody (1:200; T8660; Sigma-Aldrich) for 2 hr. All other steps, as described above, were followed to complete the ICC procedure.

Immunoblot Analysis

Three days after the axonal damage surgery, the retinas were isolated and placed into lysis buffer (10 mmol/liter Tris-HCl [pH 7.6], 100 mmol/liter NaCl, 1 mmol/liter EDTA, 1% Triton X-100, and protease inhibitors). Each sample was separated with SDS-PAGE and electroblotted onto polyvinylidene fluoride (PVDF) membranes (Millipore, Bedford, MA). After nonspecific binding had been blocked with 4% skim milk (Bio-Rad Laboratories, Hercules, CA), the membranes were incubated at 4°C overnight with a mouse monoclonal antibody against α-fodrin (1/1,000; ab11755; Abcam) and β-actin (1:2,000, F3022; Sigma-Aldrich). The membranes were then incubated with a horseradish peroxidase-conjugated mouse immunoglobulin secondary antibody, followed by avidin-biotin horseradish peroxidase complexes (Vectastain Elite ABC Kit; Vector). The signals were visualized with chemiluminescence (ECL Blotting Analysis System; Amersham, Arlington Heights, IL), measured in ImageJ software (version1.34 for Mac), and normalized to β-actin.

Statistical Analysis

The data were analyzed with the Scheffe's post hoc test followed by ANOVA or Mann-Whitney U-tests with the software EXCEL Statistics (SSRI, Tokyo, Japan). $P < 0.05$ was considered statistically significant and is highlighted in all figures with an asterisk. All values are expressed as mean ± SD.

RESULTS

To confirm axonal damage in this study, we first examined the axonal morphology. Seven days after the nerve crush or vinblastine treatments, the optic nerves around the damaged area were harvested, and the tissues were investigated by IHC with a neurofilament antibody (RT-97). The immunoreactivity of the neurofilament was homogeneously detected in untreated mice (Fig. 1A,B). In mice with a crushed optic nerve, the neurofilament immunoreactivity was disrupted just in the damaged area (Fig. 1C, arrow). The proximal part of the optic nerve appeared normal, and Wallerian degeneration occurred in the distal part of optic nerve (Fig. 1C). In the vinblastine-treated group, the axon was damaged on both the proximal and the distal parts of damaged

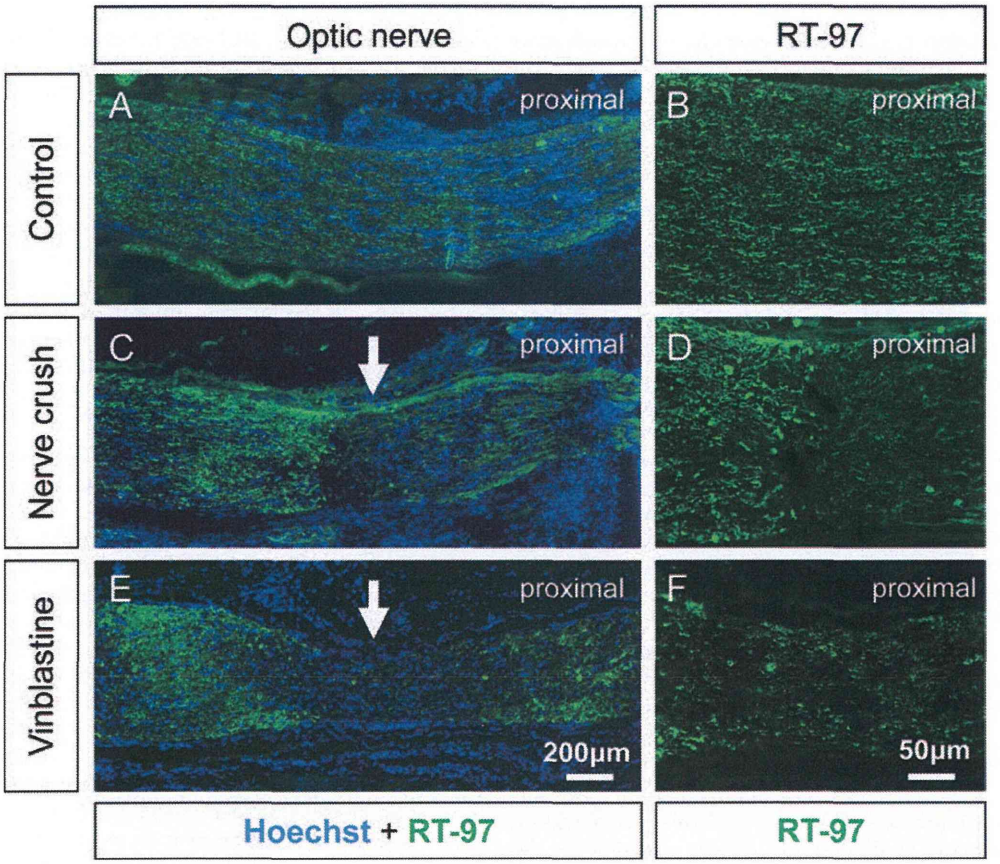

Fig. 1. Morphology of optic nerve after the axonal damage. Representative IHC photographs at lower (**A,C,E**) and higher (**B,D,F**) magnification with a neurofilament antibody (RT-97) on longitudinal optic nerve of untreated mice (A,B) and at day 7 after nerve crush (C,D) or vinblastine treatment (E,F). Arrows indicated the damage area.

area (Fig. 1E,F). Next, we investigated the axonal damage with a fluorescein tracer. We labeled RGCs by Di-I 7 days prior to the axonal damage surgery. Three days after the surgery, the RGCs were labeled again by FG (Fig. 2A). In the sham operation group (control), both Di-I and FG labels could be observed in the RGCs (Fig. 2B, upper row). However, in the axon-damaged group, only Di-I-labeled RGCs were observed and FG-labeled RGCs were not (Fig. 2B, middle and lower rows). These data suggest that both the nerve crush and vinblastine treatments induce RGC axonal damage.

To investigate the time course of RGC death following axonal damage, RGCs were labeled with FG 7 days prior to axonal damage, and the density of surviving RGCs at the various time points, 3, 7, 10, 14, and 28 days, after surgery was determined (Fig. 3A). The density of FG-labeled RGCs following optic nerve crush was 3,738 ± 308 cells/mm^2 at day 0, 3,555 ± 165 cells/mm^2 at day 3 (P = 0.100, compared with day 0), 1,153 ± 79 cells/mm^2 at day 7, 839 ± 92 cells/mm^2 at day 10, 685 ± 110 cells/mm^2 at day 14, and 488 ± 71 cells/mm^2 at day 28. From day 3 to day 7, the density of RGCs quickly decreased, and, after day 7, the density slowly decreased from day 7 to day 10. Finally, the rate of density decrease flattened out from day 10 to day 28 (Fig. 3C). The time course of the RGC death was similar in both the nerve crush and the vinblastine treatments. The density of the FG-labeled RGCs following vinblastine treatment was 3,677 ± 229 cells/mm^2 at day 0, 2,959 ± 283 cells/mm^2 at day 3 (P = 0.001, compared with day 0), 1,266 ± 139 cells/mm^2 at day 7, 837 ± 171 cells/mm^2 at day 10, 629 ± 101 cells/mm^2 at day 14, and 570 ± 78 cells/mm^2 at day 28 (Fig. 3C). On day 3 after axonal damage, the density of FG-labeled RGCs was significantly lower in the vinblastine-treated group than in the nerve crush group (P = 0.005).

To investigate the dose dependence of vinblastine on the RGC death, the density of FG-labeled RGCs was counted 7 days after surgery, treatment with vehicle, and treatment with 0.1, 1, 3, 10 mM vinblastine for each condition (Fig. 4A). Treatment with more than 1 mM vinblastine significantly induced the loss of RGC

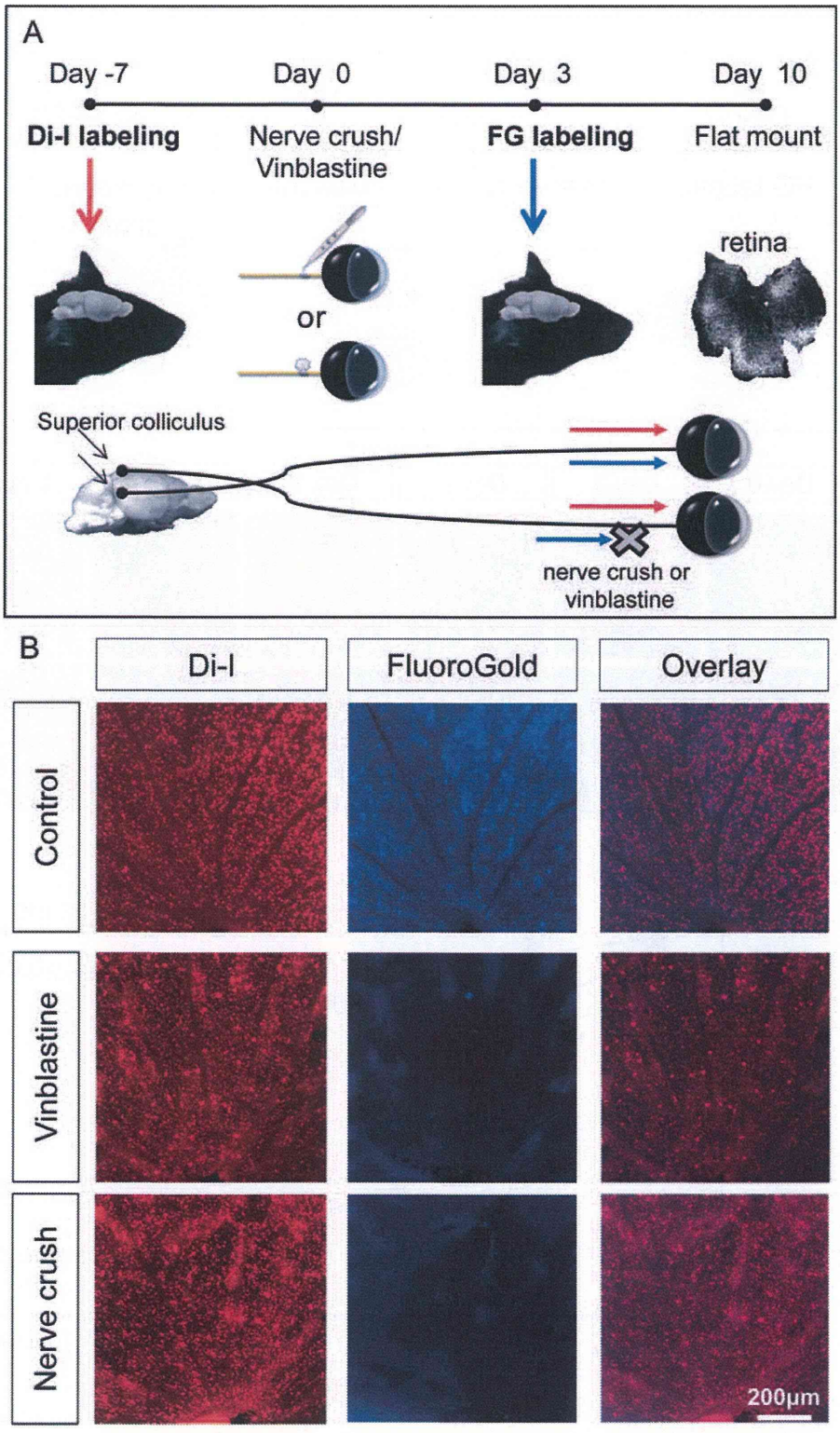

Fig. 2. Double labeling for investigation of the disturbance of axonal flow. **A:** Schematic diagram of double- and intermittent-labeling technique with two fluorescein tracers, Fluoro-Gold (FG) and Di-I. **B:** Representative results of flat-mounted retina 7 days after sham operation (upper panels) or vinblastine-treated (lower panels) from right optic nerve. In the sham operation groups (control), both the Di-I- and the FG-labeled RGCs were observed (B, upper panels). In vinblastine or nerve crush group, only Di-I-labeled RGCs were observed and FG-labeled RGCs were not (B, middle and lower panels).